Series expansions for clustering in continuum–percolation models with interactions

Asok K. Sen
Department of Mechanical and Aerospace Engineering, North Carolina State University, Raleigh, North Carolina 27695-7910

S. Torquato[a)]
Department of Mechanical and Aerospace Engineering and Department of Chemical Engineering, North Carolina State University, Raleigh, North Carolina 27695-7910

(Received 22 February 1988; accepted 3 June 1988)

The low-density expansions of the concentration of monomers, dimers, trimers, and the mean cluster size are computed exactly, up through three-body cluster integrals, for a continuum–percolation model of spheres characterized by both exclusion-volume repulsions and short-range attractions. The compactness of trimers for our model is studied in the dilute limit. Interestingly, the [1,1] Padé approximant of the mean cluster size yields percolation thresholds which exhibit the proper qualitative dependence on the strengths of the repulsive and attractive interactions. The predicted thresholds agree qualitatively well with the trends reported in a Monte Carlo study by Bug *et al.*

I. INTRODUCTION

There has been a recent upsurge of interest in the physical clusters of particles which are formed in disordered multiphase media and in liquids.[1–12] A singularly important case of physical clustering occurs at the percolation transition, the point at which a cluster becomes infinite in size. Percolation phenomena arise in a variety of applications, such as transport properties of composite materials or microemulsions, gelation, conductor–insulator transition in metals with disorder, and the glass transition. Much of the previous work regarding physical clustering has been restricted to lattice models (see the review by Essam[3]). More recently, investigators have focused their attention on the study of clustering in "continuum" models of percolation[1,2,4–12] since such models, although less tractable than their lattice counterparts, are better able to capture the essential physical aspects of real systems.

Considerable effort has been made to determine percolation thresholds, critical exponents, and the mean cluster size of continuum models using integral equation techniques,[2,6,8,9] position-space renormalization group methods,[5] and Monte Carlo simulations.[4,7,11] Except for the studies of Haan and Zwanzig[1] and Post and Glandt,[10] however, there is a dearth of work on the determination of the concentration of clusters of various sizes, cluster shapes, distribution of coordination numbers, etc.—problems which cannot be attacked using integral-equation or renormalization-group methods. Hill[13] was the first to study the extent of physical clustering of an imperfect gas in equilibrium by deriving low-density series expansions for the concentrations of various cluster sizes (monomers, dimers, trimers, etc.) in terms of the interparticle interactions. The purpose of this study is to obtain these and other series expansions for systems of particles (described below) characterized by both excluded-volume repulsions and short-range attractions. As in the work of Bug *et al.*[7] the central question is "Do interactions inhibit or enhance cluster formation?"

Haan and Zwanzig[1] obtained series expansions in density for low-order cluster concentrations, mean cluster size, and other quantities for randomly placed geometric objects of various shapes. Thus, they considered the limit in which these objects are spatially uncorrelated or are "fully penetrable" to one another. Post and Glandt[10] determined such results in the opposite limit of totally impenetrable spheres which interact with one another through a surface adhesion.[14] This model due to Baxter[14] is defined through the pair interaction

$$\beta u(r) = \begin{cases} +\infty, & 0 \leqslant r \leqslant d \\ -\ln \dfrac{\sigma}{12\tau(\sigma - d)}, & d \leqslant r \leqslant \sigma \\ 0, & r \geqslant \sigma \end{cases} \tag{1.1}$$

in the limit $d \to \sigma$. Here the parameter τ plays the role of a dimensionless temperature and σ is the diameter of a sphere. As $\tau \to \infty$, the adhesive interaction or "stickiness" vanishes and the model reduces to the simple hard-sphere fluid. Hence, the quantity τ^{-1} is the stickiness or adhesiveness.

In this paper we seek to determine low-density expansions for the concentrations of monomers, dimers, trimers, and the mean cluster size (up through three-body cluster diagrams) for a model system of spheres which incorporate exclusion-volume repulsions through the penetrable-concentric-shell (PCS)[15] model and attractive interactions through Baxter's adhesive-sphere model. In the PCS model (depicted in Fig. 1), spheres of diameter σ are statistically distributed throughout space subject only to the condition of a mutually impenetrable core of radius $\lambda\sigma/2$, $0 \leqslant \lambda \leqslant 1$. Each sphere of diameter σ, therefore, is composed of an impenetrable core of diameter $\lambda\sigma$ encompassed by a perfectly penetrable concentric shell of thickness $(1-\lambda)\sigma/2$. The extreme limits $\lambda = 0$ and $\lambda = 1$, correspond to the cases of fully penetrable (i.e., randomly centered) and totally impenetrable spheres, respectively. In this article, we superpose a Baxter-type surface adhesion on the surface of the inner hard core of radius $\lambda\sigma/2$. Note that through the same order in density, both the Haan–Zwanzig and Post–Glandt results

[a)] Author to whom all correspondence should be addressed.

 0021-9606/88/183799-09$02.10

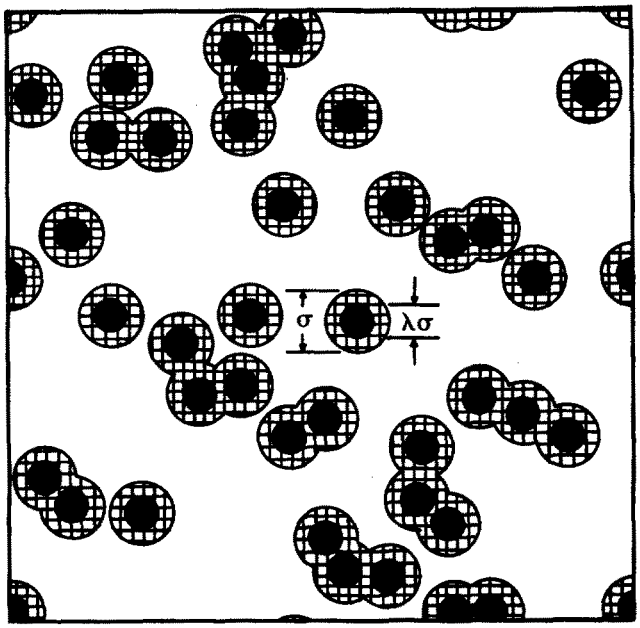

FIG. 1. A computer-generated realization of a distribution of disks of diameter σ (shaded region) in a matrix (unshaded region) in the PCS model (Ref. 15). The disks have an impenetrable core of radius $\lambda\sigma/2$ (black circular region). Here $\lambda = 0.5$ and the particle area fraction is 0.3. In the more general model of the present study, we add a Baxter-type surface adhesion on the surface of the inner hard core.

are special cases of the more general results obtained here for arbitrary λ and τ; the Haan–Zwanzig results are recovered when $\lambda = 0$ and $\tau \to \infty$ and the Post–Glandt results are recovered when $\lambda = 1$. The distance $(1-\lambda)\sigma/2$ may be thought of as the range over which an excitation may "hop" from one particle to another.[7] DeSimone *et al.*[9] have noted that the pure PCS model (without stickiness) may serve as a useful first step in studying percolation in liquid water and in liquid metals.

The rest of the paper is organized as follows. In Sec. II, we describe the general formalism to obtain expansions of the concentration of n-mers and the mean cluster size in powers of the overall particle density. In Sec. III, we discuss our model system and evaluate the first few virial coefficients for the aforementioned quantities up through three-body cluster integrals. In Sec. IV, we discuss the effect of the impenetrability parameter λ and the strength of the adhesion τ^{-1} on the concentration of n-mers and the mean cluster size. The effect of λ and τ^{-1} on the compactness of trimers in the dilute limit is examined. We also obtain the [1/1] Padé approximant from the density expansion of the mean cluster size for arbitrary λ and τ and show that the Padé approximant captures the salient features of the percolation threshold.

II. THE CLUSTER SIZE DISTRIBUTIONS AND THE PAIR CONNECTEDNESS

Using the grand canonical formalism, Hill[13] was the first to describe physical clusters in terms of "effective" potentials between bound and unbound particles. Specifically, in the notation of Coniglio *et al.*,[2] we decompose the Boltzmann factor $e(r) = \exp[-u(r)/kT]$ for the system into two contributions:

$$e(r) = e^{+}(r) + e^{*}(r), \tag{2.1}$$

where

$$e^{+}(r) = \exp[-u^{+}(r)/kT]$$

and

$$e^{*}(r) = \exp[-u^{*}(r)/kT].$$

Here u^{+} and u^{*} are the effective potentials associated with bound and unbound pairs of particles, respectively, k is the Boltzmann constant, and T is the absolute temperature. The Mayer function $f(r) = e(r) - 1$ of the system can also be separated into contributions for bound and unbound pairs:

$$f(r) = f^{+}(r) + f^{*}(r), \tag{2.2}$$

where

$$f^{*}(r) = e^{*}(r) - 1 \tag{2.3}$$

and

$$f^{+}(r) = e^{+}(r). \tag{2.4}$$

When Eq. (2.1) is used in the expression for the grand canonical partition function, one may obtain its fugacity expansion. From this quantity, one may obtain the equilibrium concentration of n-mers, ρ_n, as a power series in the number density[13,16] $\rho = N/V$, where N is the total number of particles in the system and V is the volume of the system. The density expansion for the cluster size distribution is written as

$$\rho_n = \sum_{j=n}^{\infty} B_{j,n}\rho^{j} \tag{2.5}$$

under the constraint that

$$\rho = \sum_{n=1}^{\infty} n\rho_n. \tag{2.6}$$

The latter follows from the requirement that the total number of particles in the system is a sum of the number of particles in each physical cluster. Equation (2.6) holds in the presence of finite clusters only (i.e., below the percolation threshold).

In the following diagrammatic representations of cluster integrals, let a black circle represent a ρ point whose coordinates have to be integrated over, a white circle be a root point, a full line represent $f^{+}(r)$ and a wavy line $f^{*}(r)$. Then the densities of monomers, dimers, and trimers are given by[13,16]

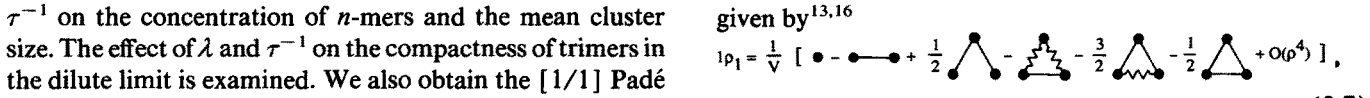

(2.7)

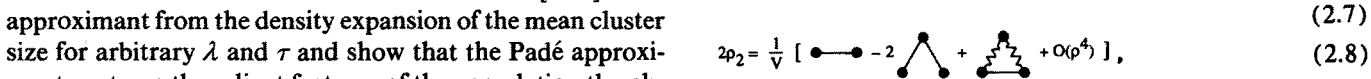

(2.8)

(2.9)

Note that the graphs presented in this paper do not contain any implicit symmetry factor. Higher-order terms ($n \geqslant 4$) may be obtained using diagrammatic analysis of Stell.[17]

The mean cluster size[18] is given by

$$S(\rho) = \frac{\sum_{n=1}^{\infty} n^2\rho_n}{\rho}. \tag{2.10}$$

Clearly, S becomes infinite at the percolation threshold. The

mean cluster size can be alternately defined in terms of the pair-connectedness function, $g^+(r)$. This function is defined[2] such that $\rho^2 g^+(\mathbf{r}_1,\mathbf{r}_2)d\mathbf{r}_1\, d\mathbf{r}_2$ is the probability that two particles within the volume elements $d\mathbf{r}_1$ and $d\mathbf{r}_2$ around $\mathbf{r}_1$ and $\mathbf{r}_2$, respectively, are physically connected. The pair-connectedness function may be obtained from a decomposition of the pair correlation function $g(\mathbf{r}_1,\mathbf{r}_2)$ into "connected" and "disconnected" contributions. For any isotropic system, the pair or radial distribution function is decomposed as[2]

$$g(r) = g^+(r) + g^*(r), \tag{2.11}$$

where $g^+(r)$ is defined to consist of all the graphs of the density expansion of $g(r)$ containing at least one path of f^+ bonds between the root points separated by the distance r. The remaining terms define the blocking function $g^*(r)$. Coniglio *et al.*[2] have shown that the mean cluster size is related to the pair connectedness by

$$S(\rho) = 1 + \rho \int g^+(r)\, d\mathbf{r}. \tag{2.12}$$

The pair-connectedness function expanded through first order in ρ is given by

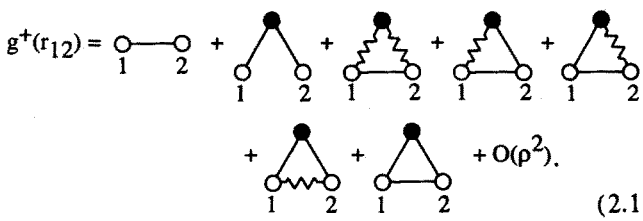

(2.13)

Substitution of Eq. (2.13) into Eq. (2.12) gives

$$S(\rho) = \sum_{j=0}^{\infty} S_{j+1}\rho^j \tag{2.14}$$

which is equivalent to Eq. (2.10). Here $S_1 \equiv 1$. Note that we denote the nth-order density coefficient of Eq. (2.14) as S_{n+1} (instead of S_n) because the integrals associated with it are $(n+1)$-body cluster diagrams. Note also that the coefficients S_j are not independent of the density coefficients $B_{j,n}$ defined in Eq. (2.5). The relation between them may be obtained by substituting Eq. (2.5) into Eq. (2.10), which leads to

$$\begin{aligned} S(\rho) &= \sum_{n=1}^{\infty}\sum_{j=1}^{\infty} n^2 B_{j,n}\rho^{j-1} \\ &= \sum_{j=0}^{\infty}\sum_{n=1}^{j+1} n^2 B_{j+1,n}\rho^j. \end{aligned} \tag{2.15}$$

Comparison of Eq. (2.15) with Eq. (2.14) gives

$$S_j = \sum_{n=1}^{j} n^2 B_{j,n}. \tag{2.16}$$

In keeping with the spirit and language of the statistical mechanics of imperfect gases, we refer to the $B_{j,n}$ and S_n as the "virial" coefficients associated with the concentration of n-mers and mean cluster size, respectively.

III. MODEL SYSTEM AND ASSOCIATED CLUSTER INTEGRALS

The model we consider consists of identical spheres of diameter σ. Each sphere is made up of two parts: an inner hard core of diameter $\lambda\sigma$ and a penetrable concentric shell (PCS) of thickness $(1-\lambda)\sigma/2$. We also add a Baxter-type surface adhesion on the surface of the hard core [which replaces σ by $\lambda\sigma$ in Eq. (1.1)]. Thus, we have an attractive interaction precisely at the radius $\lambda\sigma/2$. In this model, the unbound and bound contributions to the Mayer function are, respectively,

$$f^*(r) = \begin{cases} -1, & 0 \leqslant r \leqslant \sigma \\ 0, & r > \sigma \end{cases} \tag{3.1}$$

and

$$f^+(r) = f_p^+(r) + f_\delta^+(r). \tag{3.2}$$

Here

$$f_p^+(r) = \begin{cases} 0, & 0 \leqslant r \leqslant \lambda\sigma \\ 1, & \lambda\sigma < r \leqslant \sigma \\ 0, & r > \sigma \end{cases} \tag{3.3}$$

is the contribution to the connected part of the Mayer function due to penetrability and

$$f_\delta^+(r) = \frac{\sigma}{12\tau}\delta(r-\lambda\sigma) \tag{3.4}$$

is the contribution to f^+ due to the δ-function attraction. Thus the full line, which represents an f^+ bond in the diagrams of the previous section, now consists of two parts: a full line with a letter p below it representing an f_p^+ bond and a dashed line representing an f_δ^+ bond; diagrammatically, this means

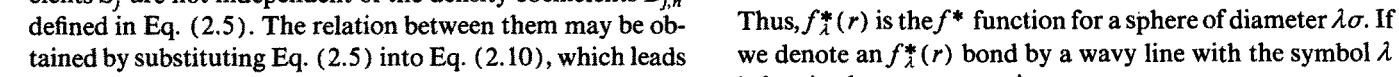

(3.5)

We remark further that f_p^+ may be written as a combination of f^* for two different spheres, as follows:

$$f_p^+(r) = f_\lambda^*(r) - f^*(r), \tag{3.6}$$

where

$$f_\lambda^*(r) = \begin{cases} -1, & 0 \leqslant r \leqslant \lambda\sigma \\ 0, & r > \lambda\sigma \end{cases}. \tag{3.7}$$

Thus, $f_\lambda^*(r)$ is the f^* function for a sphere of diameter $\lambda\sigma$. If we denote an $f_\lambda^*(r)$ bond by a wavy line with the symbol λ below it, then we may write

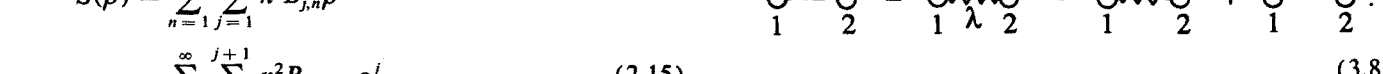

(3.8)

We now briefly describe how we compute the virial expansions for the distribution of clusters and the mean cluster size. First we replace all the full lines in expressions (2.7)–(2.9) (for the concentration of the n-mers) and expression (2.14) (for the mean cluster size) by the right-hand side of Eq. (3.8). Next the resulting cluster integrals are evaluated up to three-body graphs using the prescription outlined in the Appendix.

IV. RESULTS AND DISCUSSION

In this section, we study the effects of the impenetrability parameter λ and of stickiness τ^{-1} on the cluster size concentrations ρ_n and mean cluster size S for low densities. We

also compute a low-order Padé approximant of the series for S in order to estimate its behavior at higher densities.

For some fixed low density, we show that: (i) for nonsticky spheres ($\tau = \infty$), a decrease in λ (i.e., an increase in the thickness of the penetrable concentric shell) enhances cluster formation, as expected, and (ii) for sticky spheres (τ finite), a decrease in λ does not necessarily enhance cluster formation, i.e., in some cases, a decrease in λ will inhibit cluster formation.

For arbitrary densities, we demonstrate that (i) for nonsticky spheres, formation of very large clusters may either be enhanced or inhibited by decreasing λ, and (ii) increasing the stickiness for fixed λ does not always promote the formation of very large clusters.

A. Virial expansions

Using the procedure to evaluate cluster integrals described in the previous section, we obtain exact analytical expressions for the first few virial coefficients of series (2.5) and (2.14) for our model:

$$B_{1,1} = 1, \tag{4.1}$$

$$B_{2,1} = -V_1\left[8(1-\lambda^3) + \frac{2}{\tau}\lambda^2\right], \tag{4.2}$$

$$B_{3,1} = V_1^2\left[(32 - 96\lambda^3 + 18\lambda^4 + 46\lambda^6) + \frac{1}{\tau}(24\lambda^2 - 6\lambda^3 - 23\lambda^5) + \frac{7}{2\tau^2}\lambda^4 - \frac{1}{12\tau^3}\lambda^3\right], \tag{4.3}$$

$$B_{2,2} = V_1\left[4(1-\lambda^3) + \frac{1}{\tau}\lambda^2\right] = -\frac{1}{2}B_{2,1}, \tag{4.4}$$

$$B_{3,2} = V_1^2\left[(-49 + 96\lambda^3 + 18\lambda^4 - 65\lambda^6) - \frac{1}{\tau}\left(24\lambda^2 + 6\lambda^3 - \frac{65}{2}\lambda^5\right) - \frac{4}{\tau^2}\lambda^4\right], \tag{4.5}$$

$$B_{3,3} = V_1^2\left[(22 - 32\lambda^3 - 18\lambda^4 + 28\lambda^6) + \frac{1}{\tau}(8\lambda^2 + 6\lambda^3 - 14\lambda^5) + \frac{3}{2\tau^2}\lambda^4 + \frac{1}{36\tau^3}\lambda^3\right], \tag{4.6}$$

$$S_1 = 1, \tag{4.7}$$

$$S_2 = V_1\left[8(1-\lambda^3) + \frac{2}{\tau}\lambda^2\right] = -B_{2,1}, \tag{4.8}$$

$$S_3 = V_1^2\left[(34 - 72\lambda^4 + 38\lambda^6) + \frac{1}{\tau}(24\lambda^3 - 19\lambda^5) + \frac{1}{\tau^2}\lambda^4 + \frac{1}{6\tau^3}\lambda^3\right]. \tag{4.9}$$

Here $V_1 = \pi\sigma^3/6$ is equal to the volume of a sphere of diameter σ.

Note that in the limit of fully penetrable spheres ($\lambda = 0$), our results reduce to the Haan–Zwanzig[1] results to the same order in density (with the choice $V_1 = 1/4$). In the opposite limit of impenetrable spheres ($\lambda = 1$), we obtain the Post–Glandt[5] results (with choice $V_1 = 1$) to the same order in density. For arbitrary λ and τ, the virial expansions given above are new.

The effects of λ and τ on cluster formation are generally subtle. The case of fully penetrable spheres ($\lambda = 0$) and finite stickiness is a degenerate one, since all the results for the ρ_n and S behave as if the stickiness term is absent. The reason for this is that the adhesiveness in our model is present only on the surface of the inner hard core; but for $\lambda = 0$, this inner hard core vanishes, and hence its surface area available for cluster formation (due to surface adhesion only) is identically zero. In general, the effect of surface adhesion becomes more pronounced as the spheres become less penetrable (i.e., as λ increases). In what follows, we discuss the effects of λ and τ on the ρ_n and S in detail. Density-dependent quantities shall be expressed in terms of the reduced density $\eta = \rho\pi\sigma^3/6 = \rho V_1$.

First, we note that the second virial coefficients for ρ_1, ρ_2, and $S(\rho)$ are equivalent except for some constant multiplying factors [cf. Eqs. (4.2), (4.4), and (4.8)]. The absolute value of the first term of each of these coefficients monotonically decreases to zero as impenetrability increases, but the absolute value of the second term, proportional to the stickiness, monotonically increases as λ approaches 1. Thus, in these cases, the effects of impenetrability and surface adhesion are directly competing. Consequently, $B_{2,1}$ has a minimum and $B_{2,2}$ and S_2 have maxima (for fixed τ) at

$$\lambda_m = \begin{cases} \dfrac{1}{6\tau}, & 1/6 \leqslant \tau \leqslant \infty \\ 1, & \tau < 1/6 \end{cases}. \tag{4.10}$$

The third virial coefficients for the ρ_n and S depend on λ and τ in a somewhat more complicated fashion. We present these coefficients as a function of λ (for various values of τ) in Figs. 2–5. It is seen that the third virial coefficients (as do the second virial coefficients) go to zero in the impenetrable, nonadhesive sphere limit ($\lambda = 1$, $\tau = \infty$), and each coefficient, for all τ, start from the same point at $\lambda = 0$. For nonsticky spheres ($\tau = \infty$), the absolute magnitudes of the virial coefficients have their maxima at $\lambda = 0$; i.e., the limit corresponding to fully penetrable spheres. As the strength of adhesion increases, the positions of these maxima shift from 0 to 1. One may easily obtain a quintic equation for these maxima as a function of τ.

In Figs. 6 and 7, we plot the concentration of monomers, dimers, and trimers (normalized by the overall particle density ρ) as a function of the impenetrability parameter λ for nonsticky spheres and sticky spheres (for which $\tau = 1.0$), respectively. In each figure, we give the cluster size concentration for two (low) reduced densities of $\eta = 0.01$ and 0.05. The trimer concentration in each case is so small at $\eta = 0.01$ that it is barely distinguishable from the λ axis. For non-

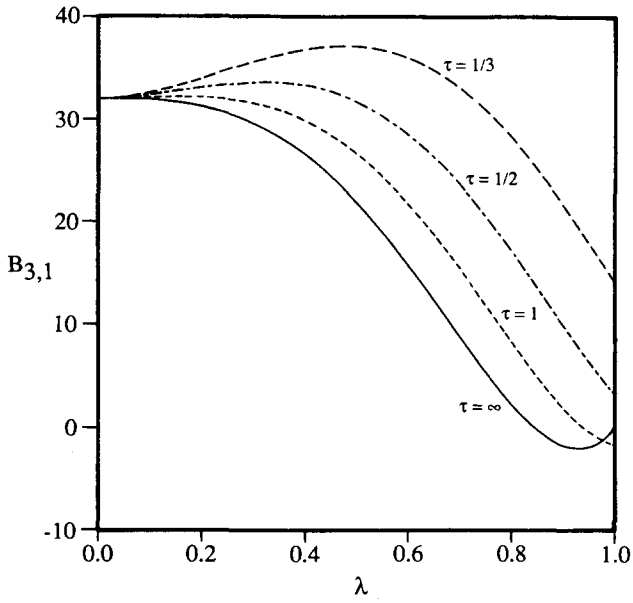

FIG. 2. The third virial coefficient $B_{3,1}$ for the monomer concentration, as a function of the impenetrability parameter λ for several values of the inverse-stickiness parameter: $\tau = \infty$, 1, 1/2, and 1/3.

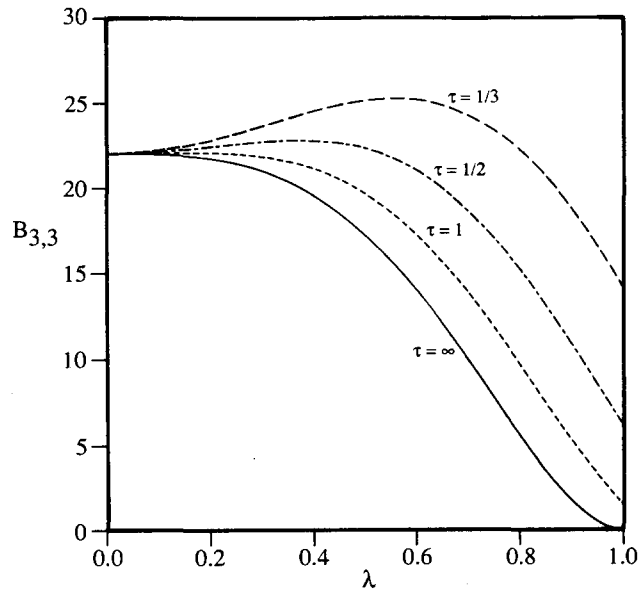

FIG. 4. As in Fig. 2 for the third virial coefficient $B_{3,3}$ for the concentration of trimers.

sticky spheres, when $\lambda = 1$, the dimer and the trimer concentration is zero and the monomer concentration equals the overall particle density at both the densities. For fixed $\lambda < 1$, as the system density increases, the concentration of higher-order clusters are expected to increase at the cost of a decrease in the monomer concentration. This is borne out in Figs. 6 and 7.

For a fixed density, as λ is increased, the concentrations of dimers and trimers first increase up to a maximum value and then decrease as λ is increased further, provided the maximum occurs for $\lambda < 1$. For nonsticky spheres at a reduced density of 0.01 (Fig. 6), this maximum for dimers occurs at a $\lambda \approx 0.0$. At a reduced density of 0.05, the same maximum occurs at a $\lambda \approx 0.62$. Through third order in density, ρ_3 for nonsticky spheres monotonically decreases with increasing λ for both $\eta = 0.01$ and 0.05. For a stickiness $\tau^{-1} = 1.0$, the maxima for dimers occur at $\lambda = 0.16$ and at 0.78, for $\eta = 0.01$ and 0.05, respectively. For the same stickiness, the trimer concentration is maximum at $\lambda \approx 0.18$ independent of η. The explanation for these observations becomes clearer by invoking the constraint relation (2.6). We have exactly, through third order in density, that

$$\rho_1 + 2\rho_2 + 3\rho_3 = \rho + O(\rho^4)$$
$$= \text{constant (for a fixed } \rho). \qquad (4.11)$$

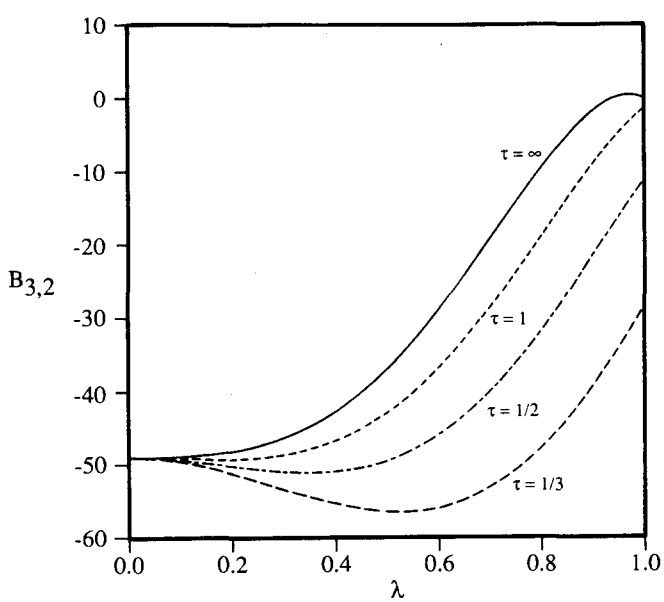

FIG. 3. As in Fig. 2 for the third virial coefficient $B_{3,2}$ for the concentration of dimers.

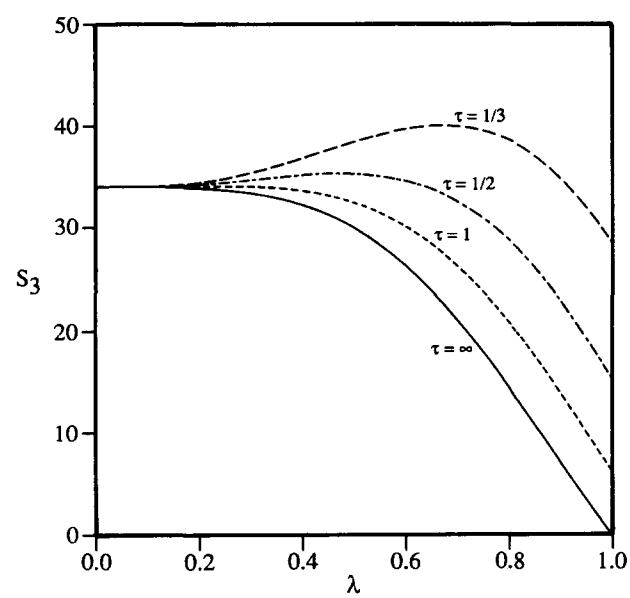

FIG. 5. As in Fig. 2 for the third virial coefficient S_3 for the mean cluster size.

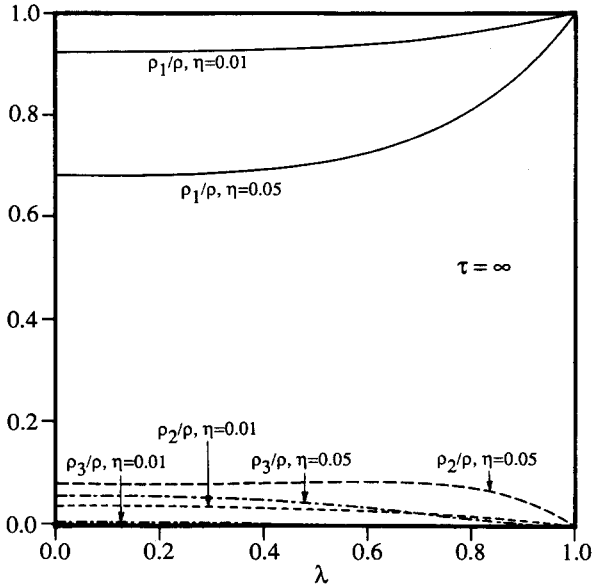

FIG. 6. Normalized n-mer concentrations (ρ_n/ρ, $n = 1,2,3$) for nonsticky spheres ($\tau = \infty$) as a function of impenetrability parameter λ. Each n-mer concentration is shown at two different reduced densities $\eta = \pi\sigma^3\rho/6 = 0.01$ and 0.05.

For nonsticky spheres, as λ is increased, the probability of forming the largest finite-sized cluster (trimer in this case) must decrease monotonically. Now since the rate at which dimers break up into monomers initially is less than the rate at which trimers break up into dimers and monomers, ρ_2 initially increases until some maximum value and then decreases beyond this value of λ because of exclusion-volume effects. In the case of sticky spheres, on the other hand, even though the constraint relation (4.11) still holds, the behavior of ρ_3 is not as simple as in the case $\tau = \infty$, since now increasing the stickiness may enhance the formation of trimers for a range of λ; thus, for fixed λ, ρ_3 goes through a maximum as discussed earlier.

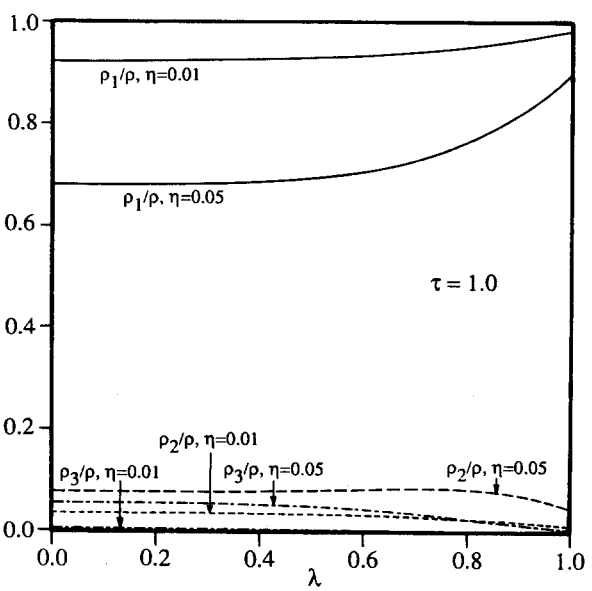

FIG. 7. As in Fig. 6 for sticky spheres with $\tau = 1$.

Figures 8 and 9 show the mean cluster size $S(\eta)$ as a function of reduced density (up to $\eta = 0.2$) for two different values of τ, at various λ. $S(\eta)$, in each case, is always monotonically increasing with increasing η. Figure 8 shows results for the pure PCS model without stickiness. The mean cluster size remains unity for all densities in the impenetrable-sphere limit. Figure 8 also demonstrates that the mean cluster size, for a given value of η, increases monotonically as $\lambda \to 0$. At low densities this result is expected on the grounds that the probability of pairwise overlap increases as $\lambda \to 0$. It is noteworthy that the mean cluster size, at a fixed density, changes by a very small amount (on the scale of our figure) as one changes the hard-core diameter from zero to a value up to about a quarter of the full diameter (σ) of the spheres. For λ as high as 1/2, the mean cluster size lies much closer to the corresponding quantity for $\lambda = 0$ than to unity (i.e., S for $\lambda = 1$). This indicates that the percolation threshold should not change significantly in the range of $0 \leqslant \lambda < 1/2$—an observation confirmed by Monte Carlo calculations.[7]

For nonzero λ, the mean cluster size $S(\eta)$, at fixed η, increases as the stickiness τ^{-1} increases. In Fig. 9, we plot $S(\eta)$ for $\tau = 1/3$. It is important to note that as the impenetratibility parameter λ is increased from zero (i.e., the value for fully penetrable spheres) at fixed η, the mean cluster size first increases with increasing λ (until a value $\lambda \approx 0.5$) and then decreases slowly until it again crosses the point for $\lambda = 0$. This nonmonotonic dependence on λ is explained as follows. For fixed but finite τ, stickiness has no effect on cluster formation when the particles are fully penetrable ($\lambda = 0$) for reasons mentioned earlier. As λ increases slightly from zero, therefore, the effect of stickiness will serve to increase S because of the finite surface area available (on the inner hard core) for adhesion. As λ increases further, S will increase (since the surface area of the inner hard core increases) until the effects of impenetrability of the inner hard

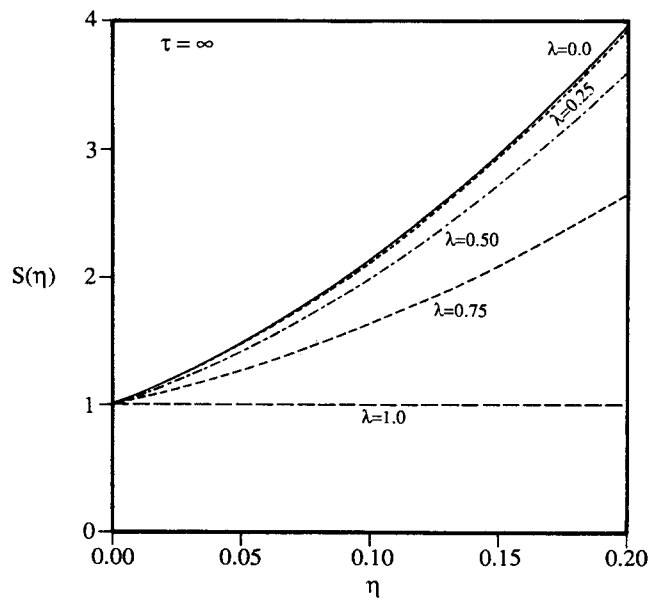

FIG. 8. Mean cluster size $S(\eta)$ for nonsticky spheres as a function of reduced density η for five different values of the impenetrability parameter: $\lambda = 0.0$, 0.25, 0.50, 0.75, and 1.0.

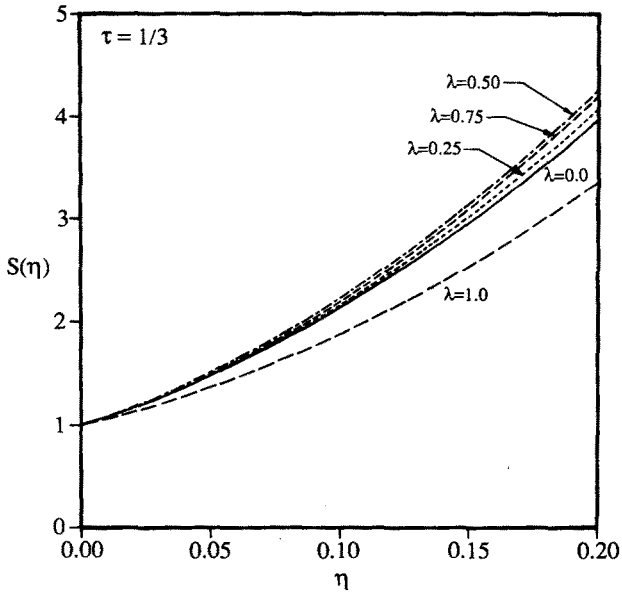

FIG. 9. As in Fig. 8 for sticky spheres with $\tau = 1/3$.

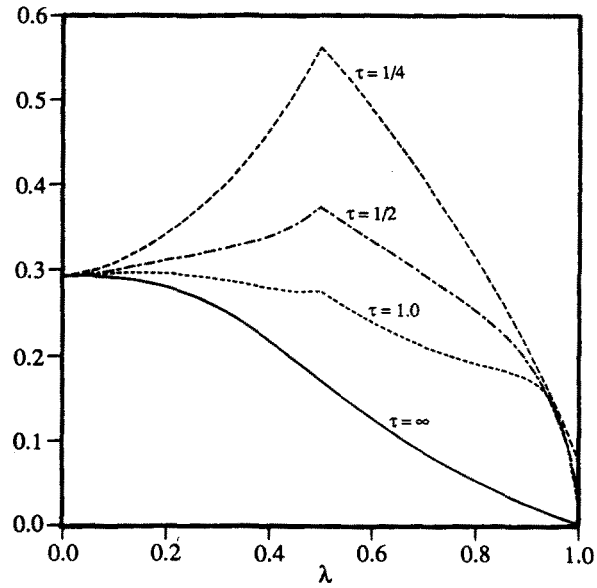

FIG. 10. Ratio of the concentration of cyclic trimers to the concentration of linear trimers in the zero-density limit as a function of the impenetrability parameter λ for given values of the inverse stickiness: $\tau = \infty$, 1, 1/2, and 1/4.

core predominate over surface adhesion effects. At this point, increasing λ, decreases S until the impenetrable-sphere limit ($\lambda = 1$) is reached.

As described in the Introduction, the advantage of studying cluster formation using a virial analysis is that it enables one to obtain a complete description of the microstructure of dilute systems. For example, using the results given above we can study the compactness of particle clusters.[10] Specifically, we consider, as a measure of the compactness of trimers, the ratio of the concentration of cyclic trimers to the concentration of linear trimers in the zero-density limit, i.e., the ratio of the third term to the sum of the first two terms in Eq. (2.9). In Fig. 10 we show this ratio as a function of the impenetrability parameter λ for given values of τ. For reasons given earlier, all the curves of Fig. 10 have the same value for $\lambda = 0$. For nonsticky spheres, the number of cyclic trimers decreases monotonically and smoothly with increasing λ. For sticky spheres (finite τ), this measure of compactness has a nonmonotonic dependence on λ, i.e., because of the competition between repulsive and attractive forces, it first increases with increasing λ (from its fully penetrable limit) until it reaches some maximum value and then decreases upon increasing λ further. Note that for finite τ, the ratio of cyclic trimers to linear trimers has a discontinuous first derivative at $\lambda = 1/2$. This cusp arises in cluster diagrams which contain at least one delta-function bond and can be explained geometrically using arguments similar to ones used by Torquato[20] to explain such behavior in related integrals.

It must be kept in mind that the results described thus far apply only to low-density situations. For arbitrary densities, the effects of λ and τ on cluster formation are expected to be even more complex.

B. [1,1] Padé approximant for the mean cluster size

In order to estimate the behavior of the mean cluster size at arbitrary density, we consider obtaining the [1,1] Padé approximate of the density expansion of S for our model. Although a [1,1] Padé approximant cannot be expected to be quantitatively accurate, we shall show that it does capture the essential qualitative features of S, even in the vicinity of percolation transition.

Now, the [1,1] Padé approximant of the mean cluster size is given by

$$S(\eta) = \frac{a - b\eta}{c - d\eta}, \tag{4.12}$$

where

$$a = c = 8(1-\lambda^3) + \frac{2\lambda^2}{\tau}, \tag{4.13}$$

$$b = -30 + 128\lambda^3 - 72\lambda^4 - 26\lambda^6 + \frac{1}{\tau} \times(-32\lambda^2 + 24\lambda^3 + 13\lambda^5) - 3\frac{\lambda^4}{\tau^2} + \frac{1}{6}\frac{\lambda^3}{\tau^3}, \tag{4.14}$$

and

$$d = 34 - 72\lambda^4 + 38\lambda^6 + \frac{1}{\tau}(24\lambda^3 - 19\lambda^5) + \frac{\lambda^4}{\tau^2} + \frac{1}{6}\frac{\lambda^3}{\tau^3}. \tag{4.15}$$

At the percolation threshold (η_P), $S(\eta)$ diverges and hence we obtain

$$\eta_P = \frac{8(1-\lambda^3) + (2\lambda^2/\tau)}{34 - 72\lambda^4 + 38\lambda^6 + (1/\tau)(24\lambda^3 - 19\lambda^5) + (\lambda^4/\tau^2) + \frac{1}{6}(\lambda^3/\tau^3)}. \tag{4.16}$$

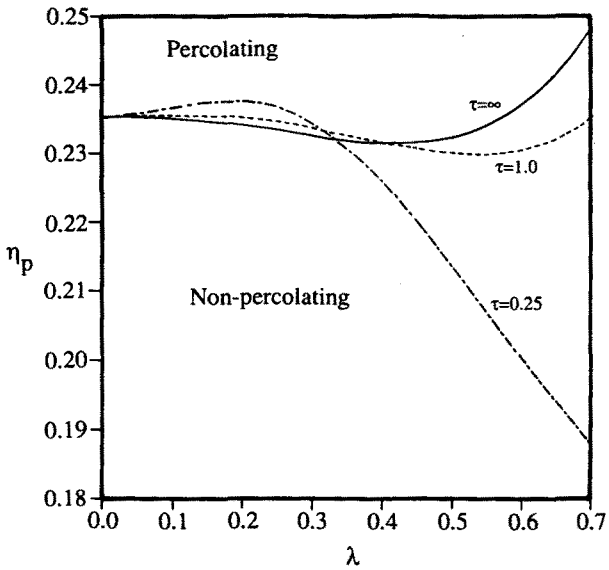

FIG. 11. Percolation threshold η_p [as obtained from [1,1] Padé approximant of mean cluster size (4.12)] as a function of impenetrability parameter λ for nonsticky spheres ($\tau = \infty$) and two other strengths of interaction, $\tau = 1.0$ and 0.25. These graphs clearly depict (qualitatively) that an attractive interaction need not always reduce the percolation threshold.

In Fig. 11, we plot the locus of the percolation line on the η_p–λ plane for $\tau = 0.25$, 1, and ∞. First consider the case of nonsticky spheres ($\tau = \infty$). Note that η_p does not monotonically increase with increasing λ. There are two competing effects operating here: (i) as λ increases (i.e., as the thickness of the penetrable concentric shell becomes smaller), the probability of two particles overlapping decreases, thus, the coordination number decreases and the percolation threshold increases, and (ii) as λ increases, for a given cluster size, the presence of the inner hard core results in clusters that occupy a larger volume of space and hence the percolation threshold decreases. For small λ, effect (ii) predominates over effect (i), but not by much, and as a result η_p decreases weakly with λ for a wide range of λ until it reaches a minimum value $\lambda_{\min} \cong 0.42$. For $\lambda > \lambda_{\min}$, effect (i) predominates and η_p increases with increasing λ. These effects are consistent with those observed by DiSimone *et al.*[9] using the Percus–Yevick approximation for the PCS model. Interestingly, our rather crude results agree qualitatively well with the Monte Carlo (MC) simulations of Bug *et al.*[7] Comparison to the Percus–Yevick (PY) approximation for the PCS model[9] reveals that although the PY solution predicts a nonmonotonic dependence on λ, it predicts a much steeper descent in η_p vs λ for small λ than either our or the MC results. The value of $\lambda_{\min} \cong 0.7$ obtained in the PY approximation matches the MC result of about 0.76 rather closely though, whereas our result underestimates the MC result by about 45%. A look at Table I shows that the PY approximation consistently overestimates the MC percolation-threshold value[21]; this is to be contrasted with the fact that our results always underestimate the MC results for η_p. Nonetheless, Eq. (4.16), derived from a [1,1] Padé approximant of S, provides a better estimate of η_p than does the PY approximation for $0 \leqslant \lambda < 0.3$ and for λ very near unity; for λ between 0.3 and very near one, the PY prediction is more accurate. It is expected that a higher-order Padé approximant, such as [2,2] approximant, would give a good estimate of η_p over the entire range of λ; however, higher-order cluster integrals become increasingly complex, and hence more difficult to evaluate, as the order increases.

TABLE I. Comparison of percolation thresholds for nonsticky spheres for several values of the impenetrability parameter λ as obtained from [1,1] Padé in the present work, Monte Carlo (MC) calculations (Ref. 7) and Percus–Yevick (PY) approximation (Refs. 6 and 9).

Impenetrability parameter λ	Reduced density at percolation η_p		
	Eq. (4.16)	MC	PY
0.0	0.24	0.35	0.50
0.54	0.23	0.34	0.41
0.90	0.31	0.40	0.44
1.0	0.40	0.64	∞

For finite τ, Fig 11 shows that increasing attractive forces does not necessarily lower the percolation threshold. For $\lambda < 0.3$, increasing the stickiness τ^{-1} actually increases the percolation threshold because clusters, for such small λ, become more compact. This effect is similar to effect (ii) described above for the pure PCS model. For $\lambda > 0.5$, increasing the adhesiveness decreases the threshold since the probability of two particles overlapping increases and hence such behavior is related to effect (i) for the pure PCS model. The results shown in Fig. 11 for finite τ agree qualitatively well with the trends seen by Bug *et al.* for a different but related model.

ACKNOWLEDGMENT

The authors gratefully acknowledge the support of the Office of Basic Energy Sciences, U.S. Department of Energy, under Grant No. DEFG05-86ER13482.

APPENDIX: EVALUATION OF THREE-BODY CLUSTER INTEGRALS

We describe a general prescription to exactly compute three-body cluster diagrams. (We do not describe evaluation of two-body diagrams, since they are easily obtained). A typical third-order graph has the form

$$\int d\mathbf{r}_{12}\, r_{12}^2\, f_1(r_{12}) \int d\mathbf{r}_{13}\, f_2(r_{13}) f_3(r_{32}), \tag{A1}$$

where the f_i could be any of the functions $f^*(r)$, $f_\lambda^*(r)$, or $\delta(r - \lambda\sigma)$ described in the text. When neither f_2 nor f_3 contains a delta function, the second integral in Eq. (A1) is given by the intersection volume $V_2^{\text{int}}(r_{12}; R_1, R_2)$ of two spheres of radii R_1 and R_2. This quantity is given by Torquato.[19] In our case, R_1 and R_2 may both be σ and/or $\lambda\sigma$. If delta functions appear in f_2 and f_3, we may use the following results:

$$\int d\mathbf{r}_{13}\,\delta(r_{13}-R_1)H(R-r_{23})$$

$$=\begin{cases}4\pi R_1^2, & 0\leqslant r_{12}\leqslant \max[0,(R-R_1)]\\ \dfrac{\pi}{r_{12}}R_1(R^2-R_1^2)+2\pi R_1^2\left(1-\dfrac{r_{12}}{2R_1}\right), & \max[0,(R-R_1)]\leqslant r_{12}\leqslant (R+R_1)\\ 0, & r_{12}>(R+R_1)\end{cases} \tag{A2}$$

and

$$\int d\mathbf{r}_{13}\,\delta(r_{13}-R_1)\delta(r_{23}-R_2)=\begin{cases}\dfrac{2\pi R_1R_2}{r_{12}}, & 0\leqslant r\leqslant (R_1+R_2)\\ 0, & r>(R_1+R_2)\end{cases}. \tag{A3}$$

In Eq. (A2), $H(x)$ is the Heaviside unit function: $H(x)=0$ if $x<0$ and $H(x)=1$ if $x>0$. Once we use Eq. (A2) or (A3) in Eq. (A1), the rest becomes a one-dimensional integral and is quite straightforward to calculate.

[1] S. W. Haan and R. Zwanzig, J. Phys. A **10**, 1547 (1977).
[2] A. Coniglio, U. DeAngelis, A. Forlani, and G. Lauro, J. Phys. A **10**, 219 (1977); A. Coniglio, U. DeAngelis, and A. Forlani *ibid.* **10**, 1123 (1977).
[3] J. W. Essam, Rep. Prog. Phys. **43**, 833 (1980).
[4] E. T. Gawlinski and H. E. Stanley, J. Phys. A **14**, L 291 (1981).
[5] E. T. Gawlinski and S. Redner, J. Phys. A **16**, 1063 (1983).
[6] Y. C. Chiew and E. D. Glandt, J. Phys. A **16**, 2599 (1983); G. Stell, *ibid.* **17**, L855 (1984); Y. C. Chiew, G. Stell, and E. D. Glandt, J. Chem. Phys. **83**, 761 (1985).
[7] A. L. R. Bug, S. A. Safran, G. S. Grest, and I. Webman, Phys. Rev. Lett. **55**, 1896 (1985).
[8] S. C. Netemeyer and E. D. Glandt, J. Chem. Phys. **85**, 6054 (1986).
[9] T. DeSimone, R. M. Stratt, and S. Demoulini, Phys. Rev. Lett. **56**, 1140 (1986); T. DeSimone, S. Demoulini, and R. M. Stratt, J. Chem. Phys. **85**, 391 (1986).
[10] A. J. Post and E. D. Glandt, J. Chem. Phys. **84**, 4585 (1986).
[11] E. M. Sevick, P. A. Monson, and J. M. Ottino, J. Chem. Phys. **88**, 1198 (1988).
[12] S. Torquato, J D. Beasley, and Y. C. Chiew, J. Chem. Phys. **88**, 6540 (1988).
[13] T. L. Hill, J. Chem. Phys. **23**, 617 (1955).
[14] R. J. Baxter, J. Chem. Phys. **49**, 2770 (1968).
[15] S. Torquato, J. Chem. Phys. **81**, 5079 (1984).
[16] W. H. Livingston and J. M. Phillips, Chem. Phys. Lett. **66**, 183 (1980).
[17] G. Stell, Physica **29**, 517 (1963).
[18] J. W. Essam, *Phase Transitions and Critical Phenomena*, edited by C. Domb and M. S. Green (Academic, New York, 1973), Vol. 2.
[19] S. Torquato, J. Chem. Phys. **84**, 6345 (1986).
[20] S. Torquato, J. Chem. Phys. **85**, 4622 (1986).
[21] The treatment of continuum percolation using the Percus–Yevick approximation, nevertheless, has its advantages. The mixed success of PY theory has been described in some depth in Refs. 6, 8, and 9.